High Density and High ρR Fuel Assembly for Fast-Ignition Inertial Confinement Fusion

Introduction

In direct-drive inertial confinement fusion,[1] a cryogenic shell of deuterium and tritium (DT) filled with DT gas is accelerated inward by direct laser irradiation (direct drive). The energy gain G is defined as the ratio between the thermonuclear energy yield and the laser energy on target. The gain is directly related to the capsule implosion velocity $G = \left(1/V_I^2\right)\eta_h \theta E_f / m_i$, where V_I is the implosion velocity, $\eta_h = E_K/E_L$ is the hydrodynamic efficiency representing the ratio between the shell kinetic energy and the laser energy on target, E_f = 17.6 MeV is the energy of the fusion products for a DT fusion reaction, and $m_i = 2.5\, m_H$ is the average ion mass. The function θ represents the fraction of burned fuel depending on the fuel areal density $\rho R \equiv \int_0^R \rho dr$. The function $\theta = \theta(\rho R)$ is commonly approximated[1] by $\theta \simeq \left(1 + 7/\rho R\right)^{-1}$, where ρR is given in g/cm^2. If the driver energy is kept constant, higher implosion velocities require lower masses. In this case, the effect on the ρR of a lower mass balances the effect of higher velocity, thus making ρR independent of velocity. The hydrodynamic efficiency[1] depends on the ratio between the initial M_0 and final mass M_1 of the capsule; $\eta_h \propto \left(M_1/M_0\right)\left(\ln M_1/M_0\right)^2/\left(1 - M_1/M_0\right)$. The difference $M_a = M_0 - M_1$ is the ablated mass, and the approximation $\eta_h \propto \left(M_a/M_0\right)^{0.87}$ can be used for $M_a < 0.7\, M_0$. The ablated mass is proportional to the ablation velocity V_a, the in-flight shell density $\rho_{\rm if}$, the implosion time t_I, and the ablation surface area $\sim R^2$; $\left[M_a \sim \rho_{\rm if} V_a R^2 t_I\right]$. By setting $M_0 \sim \rho_{\rm if} R^2 \Delta_{\rm if}$ ($\Delta_{\rm if}$ is the in-flight thickness) and by using the well-known scaling relation[1] $V_a \sim \alpha_{\rm if}^{3/5} I_L^{-1/5}$, where $\alpha_{\rm if}$ is the in-flight adiabat and I_L is the laser intensity, one can easily rewrite $\left(M_a/M_0\right) \sim \alpha_{\rm if}^{3/5} A_{\rm if}/V_I I_L^{1/15}$, where $A_{\rm if}$ is the in-flight aspect ratio and the relation $t_I \sim R/V_I$ has been used. Since the aspect ratio[1] scales as $A_{\rm if} \sim M_{\rm if}^2$ (where $M_{\rm if}$ is the in-flight Mach number), the final scaling of the hydro-efficiency can be easily derived by substituting $\rho_{\rm if} \sim \left(p_{\rm if}/\alpha_{\rm if}\right)^{3/5}$ into the Mach number, and[1] $p_{\rm if} \sim P_L \sim I_L^{2/3}$, where P_L is the laser-driven ablation pressure. A straightforward manipulation yields $\eta_h \sim V_I^{0.87} I_L^{-0.29}$, which compares favorably with a numerical fit obtained from 1-D hydrodynamic simulations

$$\eta_h^{\rm fit} \approx \frac{0.049}{I_{15}^{0.25}}\left[\frac{V_I\left({\rm cm/s}\right)}{3\times 10^7}\right]^{0.75}, \tag{1}$$

where I_{15} is the laser intensity in 10^{15} W/cm^2. The simulations are for ten direct-drive cryogenic targets with laser energies varying from 25 kJ to 1.5 MJ and are carried out using the 1-D code *LILAC*.[2] The targets used in the simulations are either all DT ice or wetted-foam CH(DT)$_6$ capsules with a 2-μm CH overcoat. Substituting the hydro-efficiency into the gain formula yields a thermonuclear gain that increases for the lower implosion velocities

$$G \approx \frac{73}{I_{15}^{0.25}}\left[\frac{3\times 10^7}{V_I\left({\rm cm/s}\right)}\right]^{1.25}\left(\frac{\theta}{0.2}\right). \tag{2}$$

Equation (2) shows that, if ignited, slow targets yield high gains. The energy required for ignition from a central hot spot, however, increases rapidly as the velocity decreases[3] $\left(E_{\rm ign}^{\rm hot-spot} \sim V_I^{-6}\right)$. This is because the hot-spot temperature increases with the velocity. Since the fusion cross section is a strong function of the temperature, slow targets have a relatively cold hot spot and therefore require greater energy for ignition. If the implosion velocity is below 2×10^7 cm/s, the hot spot cannot be ignited regardless of the shell energy since the radiation losses dominate the hot-spot energy balance. However, such slow targets can be optimal for fast ignition (FI) since the hot-spot size and energy decreases with the implosion velocity.

In fast ignition,[4] a relatively cold, high-density, and high-areal-density assembly of thermonuclear fuel is ignited by the external heating of a small volume of the dense fuel. The external heating is provided by fast electrons accelerated by the interaction of an ultra-intense petawatt (= 10^{15} W) laser pulse with either the coronal plasma or a solid target. The fast electrons slow down in the cold, dense fuel and release their kinetic energy through collisions with the electrons.

The electron range is measured in terms of the fuel areal density that, for a 1-MeV electron beam,[5] is about 0.4 to 0.6 g/cm^2. The igniter beam energy required for fast ignition increases inversely to the fuel density.[6] According to Ref. 6, the 1-MeV e-beam ignition energy follows the simple formula $E_{\rm ign}^{\rm fast} = 11\left(400/\rho_f\right)^{1.85}$, where ρ_f is the dense fuel density in g/cc. In order to keep the petawatt laser energy in the range of a few tens of kilojoules, the thermonuclear fuel density needs to exceed the value of about 300 g/cc. However, higher densities require higher beam intensities and a smaller beam radius;[6] $r_b\left(\mu{\rm m}\right) \simeq 15\left(400/\rho_f\right)$. Because of the difficulties in focusing the electron beam at radii less than 10 μm, fuel densities within the 300 to 500 g/cc range are desirable. In addition to the density range, fast ignition requires that the volume of the hot spot be much smaller than the dense core volume to reduce the thermal energy of the hot spot in favor of the internal energy of the compressed fuel. Furthermore, a small-size hot spot limits the detrimental effects of the central low-density plasma on the burn wave propagation that starts in the dense volume. Other fuel-assembly requirements come from the specific applications of FI. For inertial fusion energy (IFE) applications, the thermonuclear gain must be greater than 100 and the areal density must be at least 2.5 to 3 g/cm^2. Here we show that a fuel assembly meeting all these requirements can be produced with a direct-drive laser facility in the 700 kJ range, about half the size of the National Ignition Facility[7] and significantly smaller than the multimegajoule drivers required for direct-drive IFE based on hot-spot ignition.

Scaling Laws for Density, Areal Density, and Stagnation Aspect Ratio

We start our analysis by deriving a scaling law for the shell density, areal density, and hot-spot size as a function of characteristic implosion parameters such as shell energy, implosion velocity, and in-flight adiabat. By indicating with Δ_s the stagnating shell thickness, with R_h the hot-spot radius and M_s the shell mass, the compressed shell areal density scales as

$$\rho_s\Delta_s \sim M_s/R_h^2\Sigma\left(A_s\right) \sim E_K/R_h^2V_I^2\Sigma\left(A_s\right),$$

where E_K is the shell kinetic energy at the end of the acceleration phase, $A_s = R_h/\Delta_s$ is the stagnation aspect ratio, and $\Sigma\left(x\right) = 1 + 1/x + 1/3x^2$ is a volume factor. The hot-spot radius R_h can be derived by setting the total shell internal energy at stagnation equal to the shell kinetic energy $E_K \sim p_s\left(R_h + \Delta_s\right)^3$, where the stagnation pressure p_s has been assumed to be approximately uniform through the hot spot and shell. This energy conversion condition (from kinetic to internal) can be rewritten by setting $p_s \sim \alpha_s\rho_s^{5/3}$, where $\alpha_{\rm s}$ is the stagnation adiabat that is related[8] to the in-flight adiabat $\alpha_{\rm if}$ through the in-flight Mach number $\alpha_s \sim \alpha_{\rm if}M_{\rm if}^{2/3}$, leading to $\alpha_s \sim \alpha_{\rm if}^{0.8}V_I^{0.67}/P_L^{0.13}$. It follows that the shell density and the shell areal density can be rewritten as

$$\rho_s\Delta_s \sim \Phi\left(A_s\right)E_K^{0.33}V_I^{0.67}I_L^{0.09}\alpha_{\rm if}^{-0.8} \tag{3}$$

and

$$\rho_s \sim \Psi\left(A_s\right)V_I^2I_L^{0.13}\alpha_{\rm if}^{-1.2}, \tag{4}$$

where

$$\Phi\left(x\right) \equiv \left(x^2 + x + 1/3\right)^{2/3}/\left(1 + x\right)^3$$

and

$$\Psi\left(x\right) = \left[\Phi\left(x\right)\left(1 + x\right)\right]^{9/4}.$$

Though the stagnation aspect ratio is of order unity, it is important to accurately determine its functional dependency on the implosion parameters. For reasonable values of the stagnation aspect ratio ranging between $1 < A_s < 4$, Φ and Ψ can be approximated with a power law as $\Phi\left(A_s\right) \sim 1/A_s^{0.92}$ and $\Psi\left(A_s\right) \sim 1/A_s^{0.62}$. A_s grows with the implosion velocity since the mass decreases for a fixed energy leading to smaller Δ_s, while R_h depends mostly on energy. In order to determine an accurate dependence on the velocity, we fit the results of the simulations where R_h is defined as the point of maximum shell density, and Δ_s is the distance between R_h and the return shock at the time of peak areal density. The simulations show a clear dependence on the velocity and almost no dependence on energy and adiabat leading to

$$A_s^{\rm fit} \approx 2.1\left[\frac{V_I\left({\rm cm/s}\right)}{3 \times 10^7}\right]^{0.96}, \tag{5}$$

as shown in Fig. 103.1. Substituting Eq. (5) into (3) and (4) yields scaling laws for the density and areal density

$$\rho_s\Delta_s \sim E_L^{0.33}V_I^{0.03}\alpha_{\rm if}^{-0.8}, \quad \rho_s \sim V_I^{1.4}I_L^{0.13}\alpha_{\rm if}^{-1.2}, \tag{6}$$

where the hydro-efficiency from Eq. (1) has been used. These semi-analytical scaling laws compare favorably with the numerical fits of the peak values of the densities and areal densities

$$\left(\rho R\right)_{\max}^{\text{fit}} \approx \frac{1.3}{\alpha_{\text{if}}^{0.55}}\left[\frac{E_L\,(\text{kJ})}{100}\right]^{0.33}\left[\frac{V_I\left(\text{cm}/\text{s}\right)}{3\times 10^7}\right]^{0.06} \tag{7}$$

and

$$\rho_{\max}^{\text{fit}} \approx \frac{788}{\alpha_{\text{if}}}\, I_{15}^{0.13}\left[\frac{V_I\left(\text{cm}/\text{s}\right)}{3\times 10^7}\right], \tag{8}$$

where the subscript max indicates the maximum values during the implosion and ρR and $\rho_{\max}$ are in g/cm^2 and g/cc, respectively. The laser-intensity scaling in (8) is analytical from (6) since the intensity varies only within a ±15% range in the simulation, and it does not represent a good scaling parameter. Note the density scaling is somewhat different from the indirect-drive scaling shown in Ref. 9. The areal density in Eq. (7) includes the inner portion of the shell that has been compressed by the return shock as well as the surrounding portion that has not been shocked. Typically, the unshocked portion has significantly lower density and lower ρR with respect to the shocked portion (see Fig. 103.4 on p. 121). In a $\rho R \sim 3$ g/cm^2 implosion, however, a 20% fraction of unshocked ρR can stop energetic electrons at lower densities (with $\rho < 300$ g/cc), preventing them from reaching the dense shocked core. The presence of the unshocked areal density has important consequences on the choice of the fast-ignition time. If the fast electrons have 1-MeV energy, then the fast-ignition time is when the unshocked areal ρR is significantly less than 0.6 g/cm^2, which occurs after the time of peak ρR. This constraint is relaxed as the fast-electron energy exceeds 1 MeV. Note that Eq. (8) represents the maximum density. The time of peak ρR occurs after the time of peak density, and the average density at the time of peak ρR is slightly below 80% of Eq. (8). If fast ignition is triggered at or soon after the time of peak ρR, the corresponding average density is significantly below its maximum value.

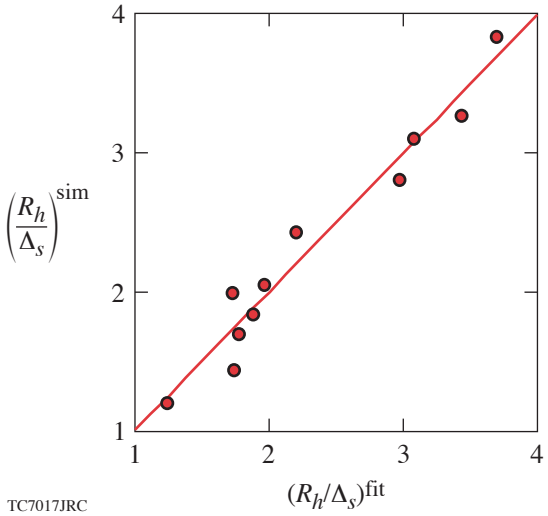

Figure 103.1
Hot-spot aspect ratio from simulation compared with numerical fit (9).

Laser Pulse Shaping

Other important considerations in optimizing fast-ignition targets concern the pulse length and laser power contrast ratio. It is clear from Eqs. (7) and (8) that low adiabat implosions lead to high densities and areal densities. However, very low adiabat implosions require long pulse lengths and careful pulse shaping. The long pulse length is because of the slow velocity of the low-adiabat shocks, and the careful shaping is required to prevent spurious shocks from changing the desired adiabat. Furthermore, the ratio between the peak power and the power in the foot of the laser pulse (i.e., the power contrast ratio) increases as the adiabat decreases thus leading to difficult technical issues in calibrating the pulse shape. These constraints on the pulse shape are relaxed by using the relaxation (RX) laser pulse technique.[10] The relaxation pulse consists of a prepulse followed by an interval of laser shutoff and the main pulse. The RX pulse induces an adiabat profile that is monotonically decreasing from the ablation surface to the inner shell surface. In addition to improving the hydrodynamic stability of the implosions, the RX main pulse is shorter and requires a lower contrast ratio than the equivalent flat adiabat pulse with the same inner surface adiabat.

High-Gain Fast-Ignition Capsule Design

By using the results in Eqs. (5), (7), and (8), a high-gain fast-ignition capsule can be designed. We start by setting a low value for the inner-surface adiabat $\alpha_{\text{if}}^{\min} \approx 0.7$. An adiabat below unity implies that, at shock breakout, the inner portion of the shell is not fully ionized. In order to achieve a $\rho R \approx 3$ g/cm^2, Eq. (7) yields a laser energy $E_L \simeq 750$ kJ [the velocity term in Eq. (7) has been ignored because of the low power index]. Equation (8) is then used to determine the velocity required to obtain a peak density of 640 g/cc that corresponds to an average density of the shocked shell at the time of peak ρR of $\langle\rho\rangle \simeq 0.8\,\rho_{\max} \simeq 500$ g/cc. The corresponding velocity from (8) is $V_I = 1.7\times 10^7$ cm/s, leading to a hot-spot aspect ratio [Eq. (5)] of $A_s \sim 1$. Since the required laser energy of 750 kJ is approximately half the NIF energy, we use a reference driver with half the energy and half the power of the NIF. For a peak power of 220 TW, the outer shell radius is chosen to keep the

peak intensity at 10^{15} W/cm^2, thus leading to $R_{out} \simeq 1.3$ mm. The target mass at stagnation is derived from the kinetic energy $M_s \approx 2E_K/V_I^2$, with $E_K \approx \eta_h E_L$. Using Eq. (1) for η_h and $E_L = 750$ kJ, $V_I \approx 1.7 \times 10^7$ cm/s yields a stagnation mass of $M_s \simeq 1.7$ mg. Assuming that ~20% of the mass is ablated leads to an initial mass of about $M_0 \simeq 2$ mg. In order to improve the laser energy absorption, we consider a wetted-foam target with an inner ice layer, an outer wetted-foam CH(DT)$_6$ layer, and a 2-μm CH overcoat. Given the low density of the foam and the small thickness of the overcoat, we can assume that the average density is the same as DT ice, $\rho_0 \simeq 0.25$ g/cc, and determine the inner-shell radius from the volume ~M_0/ρ_0 and the outer radius leading to $R_{inn} \simeq 660$ μm. Figure 103.2 shows the FI target with a foam layer thickness that is large enough to reabsorb the coronal radiation and reduce the radiation heating of the inner ice layer. It is important to notice that the large shell thickness combined with the slow implosion velocity makes the target performance insensitive to the hydrodynamic instabilities and 1-D codes suitable for realistic simulations of the implosion. The 750-kJ RX pulse is shown in Fig. 103.3. The main foot-pulse length is about 22 ns, and the power contrast ratio is about 150. Those pulse characteristics are not far from the NIF indirect-drive pulse requirements with a pulse length of ~18 ns and a contrast ratio of ~100. A *LILAC* simulation of the 750-kJ implosion yields the exact desired implosion parameters. Substituting the implosion parameters into the gain formula (1) yields a thermonuclear gain of about $G = 220/(1 + E_{PW}/750)$, where E_{PW} is the petawatt laser energy required for ignition in kilojoules. This is probably an optimistic assessment since it assumes that the peak value of the areal density is available at the time of ignition. Figure 103.4 shows the density profiles versus the areal density at different times about the peak ρR time. The sharp drops in density shown in Fig. 103.4 correspond to the return shock traveling outward from the center. Notice that the density varies significantly while the total ρR remains above 2.5 g/cm^2. Ignition can therefore be triggered at an average density varying from 300 to 550 g/cc without significant changes to the target gain. It is important to observe that the areal density of the low-density unshocked portion of the shell is significant and decreases with time from 0.9 g/cm^2 at time of $\rho R = 3$ g/cm^2 to 0.3 g/cm^2 at the time $\rho R = 2.5$ g/cm^2. This implies that the electron energy in the fast-ignitor beam needs to exceed 1 MeV to allow the electron penetration into the high-density core. The density versus volume plots in Fig. 103.5 indicate that the hot-spot volume is less than 10% of dense core during hundreds of picoseconds about the time of peak ρR. Notice that at 27.5 ns, the density is about 300 g/cc, and its profile is approximately uniform. The "hot-spot" volume is small, and values below $\rho < 300$ g/cc are confined within a tiny region occupying only 6%–7% of the core.

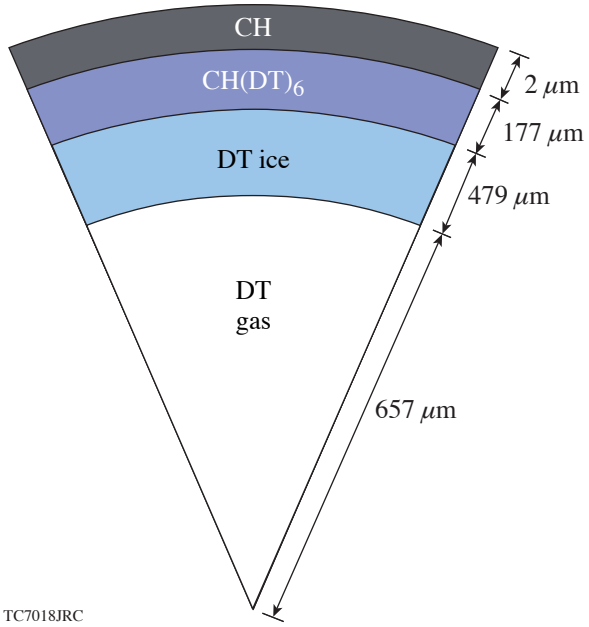

Figure 103.2
Fast-ignition IFE target.

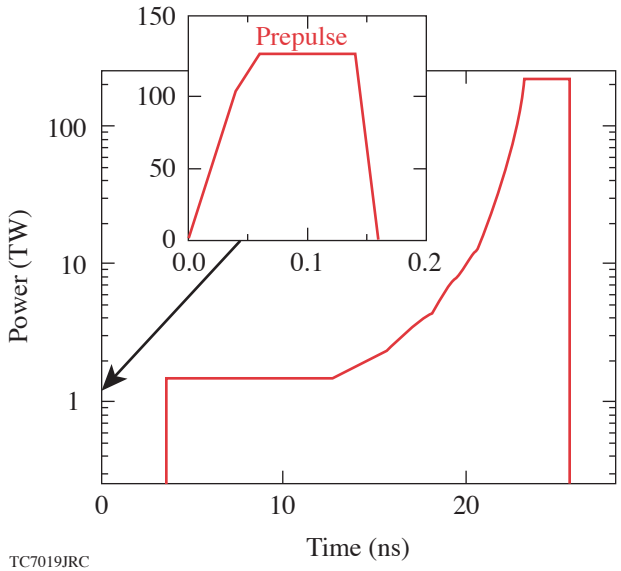

Figure 103.3
750 kJ, $\alpha = 0.7$ relaxation laser pulse.

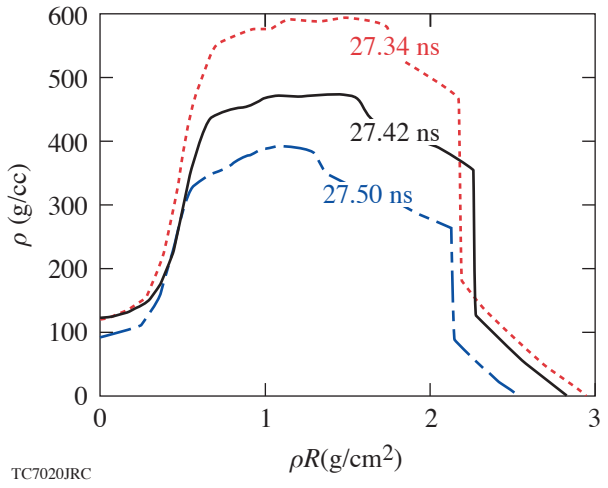

Figure 103.4
Density profiles versus areal density at three times about the time of peak areal density.

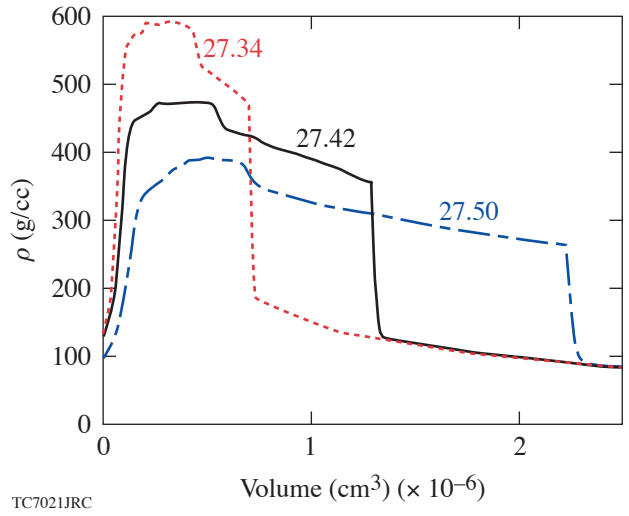

Figure 103.5
Density profiles versus volume at three times about the time of peak areal density.

ACKNOWLEDGMENT

This work has been supported by the US Department of Energy under Cooperative Agreement DE-FC02-04-ER54789 and DE-FC52-92SF19460, the University of Rochester, and the New York State Energy Research and Development Authority. The support of DOE does not constitute an endorsement by DOE of the views expressed in this article.

REFERENCES

1. S. Atzeni and J. Mer-ter-Vehn, *The Physics of Inertial Fusion: Beam Plasma Interaction, Hydrodynamics, Hot Dense Matter*, International Series of Monographs on Physics (Clarendon Press, Oxford, 2004); J. D. Lindl, *Inertial Confinement Fusion: The Quest for Ignition and Energy Gain Using Indirect Drive* (Springer-Verlag, New York, 1998).
2. J. Delettrez and E. B. Goldman, Laboratory for Laser Energetics Report No. 36, University of Rochester (1976).
3. M. C. Herrmann, M. Tabak, and J. D. Lindl, Nucl. Fusion **41**, 99 (2001).
4. M. Tabak *et al*., Phys. Plasmas **1**, 1626 (1994).
5. C. Deutsch *et al*., Phys. Rev. Lett. **77**, 2483 (1996); **85**, 1140(E) (2000); C. K. Li and R. D. Petrasso, Phys. Rev. E **70**, 067401 (2004).
6. S. Atzeni, Phys. Plasmas **6**, 3316 (1999).
7. E. M. Campbell and W. J. Hogan, Plasma Phys. Control. Fusion **41**, B39 (1999).
8. R. Betti, K. Anderson, V. N. Goncharov, R. L. McCrory, D. D. Meyerhofer, S. Skupsky, and R. P. J. Town, Phys. Plasmas **9**, 2277 (2002).
9. S. A. Slutz and M. C. Herrmann, Phys. Plasmas **10**, 234 (2003).
10. R. Betti, K. Anderson, J. Knauer, T. J. B. Collins, R. L. McCrory, P. W. McKenty, and S. Skupsky, Phys. Plasmas **12**, 042703 (2005).